Short Communication

Preparation of Nano-Ag$_4$Bi$_2$O$_5$/Graphene Oxide Composite and Study of Its Catalytic Performance for Oxygen Reduction Reaction

Dongmei Chen[1], Pingyuan Wang[2], Yanzhi Sun[2], Bixue Zhu[1,], Junqing Pan[2,*]*

[1] Key Laboratory of Macrocyclic and Supramolecular Chemistry, Guizhou University, Guiyang 550025, P.R. China
[2] State Key Laboratory of Chemical Resource Engineering, Beijing University of Chemical Technology, Beijing 10029, P.R. China
[*]E-mail: bxzhu@gzu.edu.cn; jqpan@mail.buct.edu.cn

A nano-Ag$_4$Bi$_2$O$_5$/graphene oxide (ABO/GO) composite has been synthesized by a co-precipitation method in which the ABO was homogeneously precipitated on the surface of suspended graphene oxide. The structure, morphology, composition, and electrochemical properties have been systematically investigated by XRD, Raman spectroscopy, SEM, EDS and EDX mapping, XPS, and electrochemical measurements. The results showed that ABO had been successfully loaded on GO to form an ABO/GO composite. The obtained ABO/GO hybrid exhibited excellent electrocatalytic performance for the oxygen reduction reaction (ORR). Analytical results obtained with a rotating disk electrode (RDE) showed that the ORR took place via a four-electron pathway on the surface of the ABO/GO electrocatalyst.

1. INTRODUCTION

The structure and surface characteristics of oxygen reduction catalysts, as well as the carrier material, directly influence the activity and stability of the catalyst. A nano-Ag$_4$Bi$_2$O$_5$/graphene oxide (ABO/GO) composite has been synthesized by a co-precipitation method in which ABO was precipitated on the surface of suspended GO. Compared with pure ABO and GO, the ABO/GO composite demonstrated excellent catalytic performance and stability in the ORR and the process involved a four-electron pathway.

To ensure that a catalyst retains its nanostructure and maintains adequate catalytic activity under the working conditions, the most common approach to reduce the dosage of catalyst and enhance its catalytic efficiency is to disperse it on a suitable carrier [1,2]. As an oxygen reduction catalyst carrier, graphene oxide (GO) has obvious superiority and bright prospects because of its huge specific surface area and large quantity of hydroxyl (-OH), carboxyl (-COOH), and epoxide groups on its surface, resulting in good hydrophilicity [3-5].

Recent studies have shown that metal nanoparticles, such as Au [6], Ag [7], Pd [8], Pt [9], Ni [10], and Cu [11], deposited on GO templates, not only serve to prevent agglomeration, but also increase the specific surface area of the composite. Composites of metal oxide nanoparticles and graphene oxide constitute a "hot topic" in the study of ORR catalysts. Composites consisting of metal oxide nanoparticles, such as TiO_2 [12], ZnO_2 [13], MnO_2 [14], SnO_2 [15], Fe_3O_4 [16], or Co_3O_4 [17], and graphene oxide have been the focus of attention in recent years. These composite materials greatly promote the performance of the catalysts, expanding their application fields. Khan [18] deposited metal nanoparticles on graphene templates such as Pd/GO, Pt/GO, and PdPt/GO, and the resulting catalysts displayed good ORR activity and stability.

Herein, we propose nano-$Ag_4Bi_2O_5$/graphene oxide (ABO/GO) composite as a new ORR catalyst. It was synthesized by a co-precipitation method on the surface of homogeneously suspended GO, and shows an efficient pathway for charge transfer. Compared with pure ABO and GO, the ORR performance of ABO/GO product was significantly enhanced in the alkaline electrolyte.

2. EXPERIMENT

2.1 Material synthesis

The synthetic route to the catalyst is illustrated in Scheme 1. Graphene oxide (GO, Nanjing Xianfeng Advanced Materials Ltd. Co.) was synthesized by a modified Hummers method [19,20]. $Ag_4Bi_2O_5$ (ABO)-modified GO was synthesized as follows. Firstly, KOH (38.38 g; 96%, Beijing Jingxi Chemical Reagent Ltd. Co.) was dissolved in deionized water to obtain 100 mL of 6.5 mol·L^{-1} KOH (base solution **A**) as a precipitant. GO powder was then added to the above solution and sonicated for 2 h. Ag_2O (1.16 g; AR, Beijing Jingxi Chemical Reagent Ltd. Co.) and Bi_2O_3 (1.17 g; AR, Beijing Jingxi Chemical Reagent Ltd. Co.) were dissolved in 50 mL of 1 mol·L^{-1} HNO_3 (solution **B**) as the Ag-Bi source. Under conditions of a constant temperature of 30 °C and strong agitation at 800 rpm, 50 mL of solution **B** was pumped into solution **A** at a rate of 3 mL·min^{-1}. As indicated in Scheme 1, the as-obtained ABO coating on the surface of the GO was amorphous. After crystallization for 1 h, the amorphous ABO doped on the GO had completely crystallized. The precipitated product was then washed with deionized water until the washings were neutral. Finally, the product was dried in vacuo at room temperature for 24 h to obtain the final sample. For comparison, pure ABO powder without GO was also prepared under the same conditions.
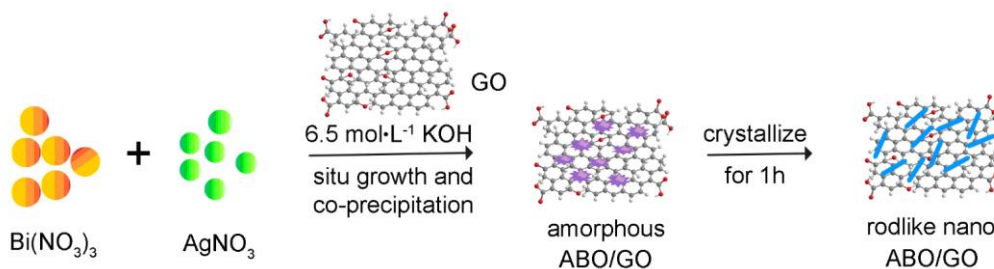
Scheme 1. Schematic representation of the synthesis of the ABO/GO

2.2 Characterizations

XRD analysis of the prepared catalysts was carried out on a Rigaku D/max 2500VB2+/PCX X-ray diffractometer. Raman spectroscopy was performed using a Thermo Fisher ESCALAB 250 spectrometer. The morphology of the synthesized samples was examined by means of a scanning electron microscope (SEM, ZEISS, SUPRA 55). Energy-dispersive X-ray spectroscopy (EDS and EDX) was carried out on a LINK-ISIS300 instrument (Oxford Instruments). X-ray photoelectron spectroscopy (XPS) was analyzed using an ULVAC-PHI Quantera SXM spectrometer. The cyclic voltammetry (CV, Shanghai Chen Hua electrochemical workstation, CHI760D) test was carried out to study the electrochemical activity and stability. The rotating disk electrode (RDE) tests were carried out with an electrochemistry workstation (PARSTAT 2273) with a three-electrode system at room temperature.

3. RESULTS AND DISCUSSION

3.1 Structural characterization of the prepared samples
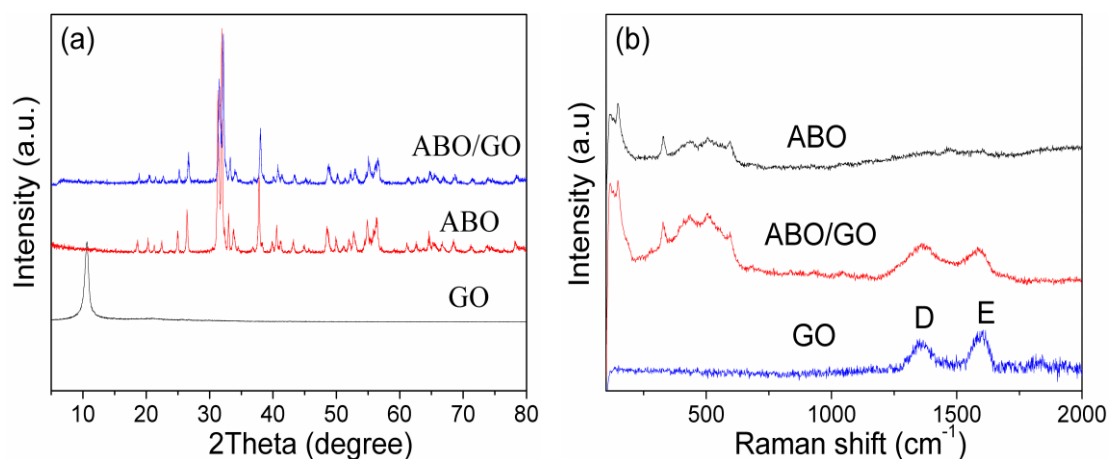
Figure 1. XRD pattern (a) and Raman pattern (b) for GO、ABO and ABO/GO

Figure 1a displays the XRD patterns of GO, ABO, and ABO/GO composite, respectively. The

strong diffraction peak located at 11.2° is assigned to (001) of GO. It can be seen that the $Ag_4Bi_2O_5$ sample showed seven strong peaks at 26.37°, 31.25°, 31.85°, 37.76°, 40.50°, 48.35°, and 54.81°, corresponding to the (112), (411), (312), (600), (420), (314), and (703) facets of the structure of $Ag_4Bi_2O_5$ (JCPDS 87-0866), respectively.
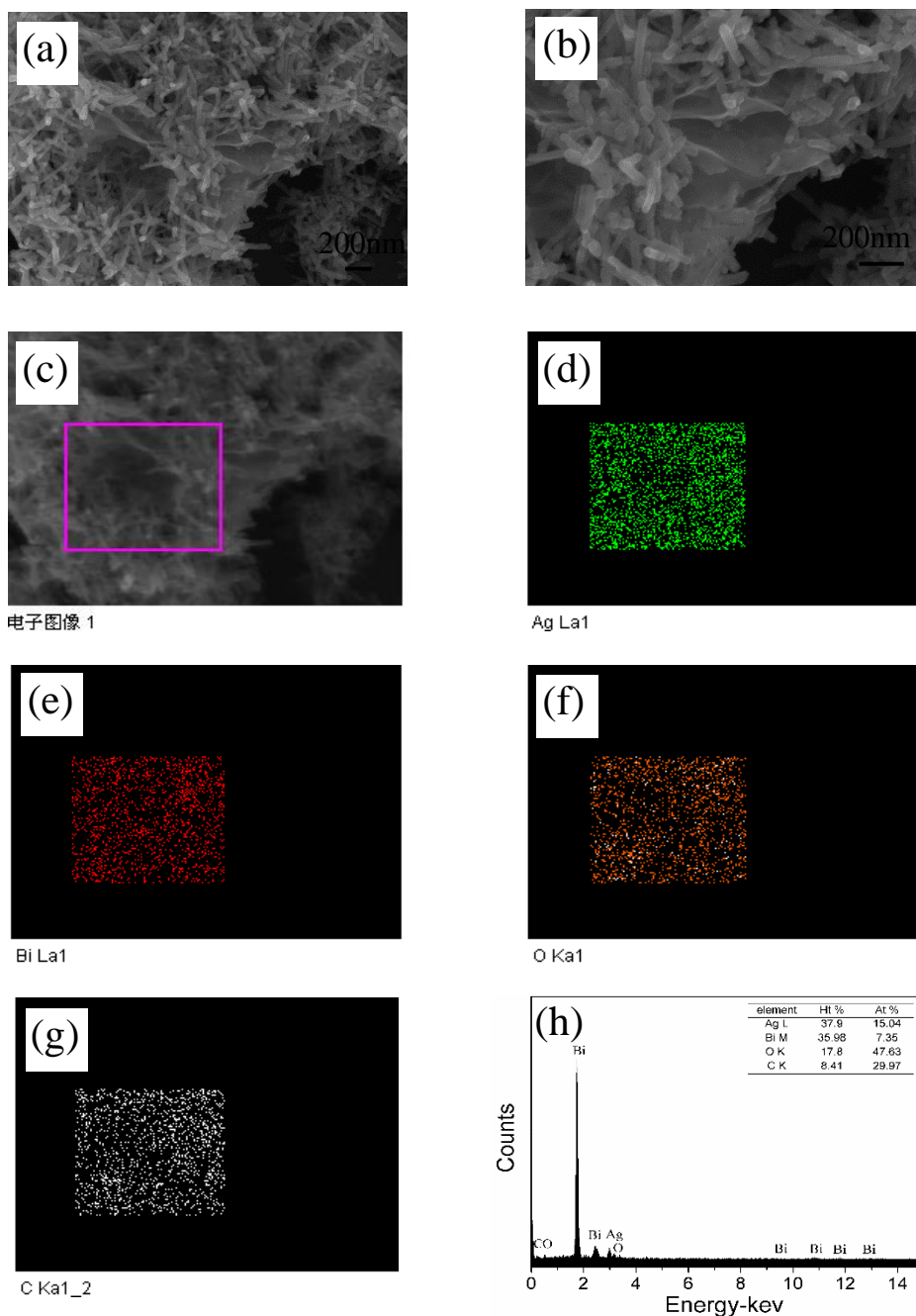

Figure 2. SEM (a, b,c), EDX elemental mapping images (e, f, g), and EDS spectrum of the ABO/GO sample (h).

After forming the ABO/GO composite, all of the characteristic peaks were broadened, indicating a decrease in the crystallinity of ABO. Raman spectroscopy is one of the most sensitive and

informative techniques for characterizing disorder in sp^2 carbon materials. Representative Raman spectra of GO, ABO, and ABO/GO are shown in Fig. 1b. As can be seen in Fig. 1b, compared to those of GO, the G-band shifted from ν=1596 to 1592 cm^{-1} and the D-band shifted from ν=1353 to 1368 cm^{-1}, which could be attributed to structural defects of GO. The Raman spectral results were in good agreement with those in previous reports [21-23]. The Raman peaks of the ABO/GO composite in the range from 100 cm^{-1} to 1000 cm^{-1} can be attributed to Ag-O and Bi-O bonds.

SEM images of the ABO/GO catalyst are shown in Fig. 2 (a)−(c), which confirm the presence of GO. In addition, a large amount of ABO-coated GO nanorods of width 20−30 nm and length 200−300 nm can be discerned. Figure 2 (d)−(g) show the analysis results of EDX mapping of the selected overall area of SEM (Fig. 2 (c)). Peaks due to silver, bismuth, carbon, and oxygen can all be clearly discerned. The contents of Ag, Bi, O, and C were calculated as 15.04 wt%, 7.35 wt%, 47.63 wt%, and 29.97 wt%, respectively, as indicated in Fig. 2 (h). These mapping images thus confirmed the presence of ABO/GO.
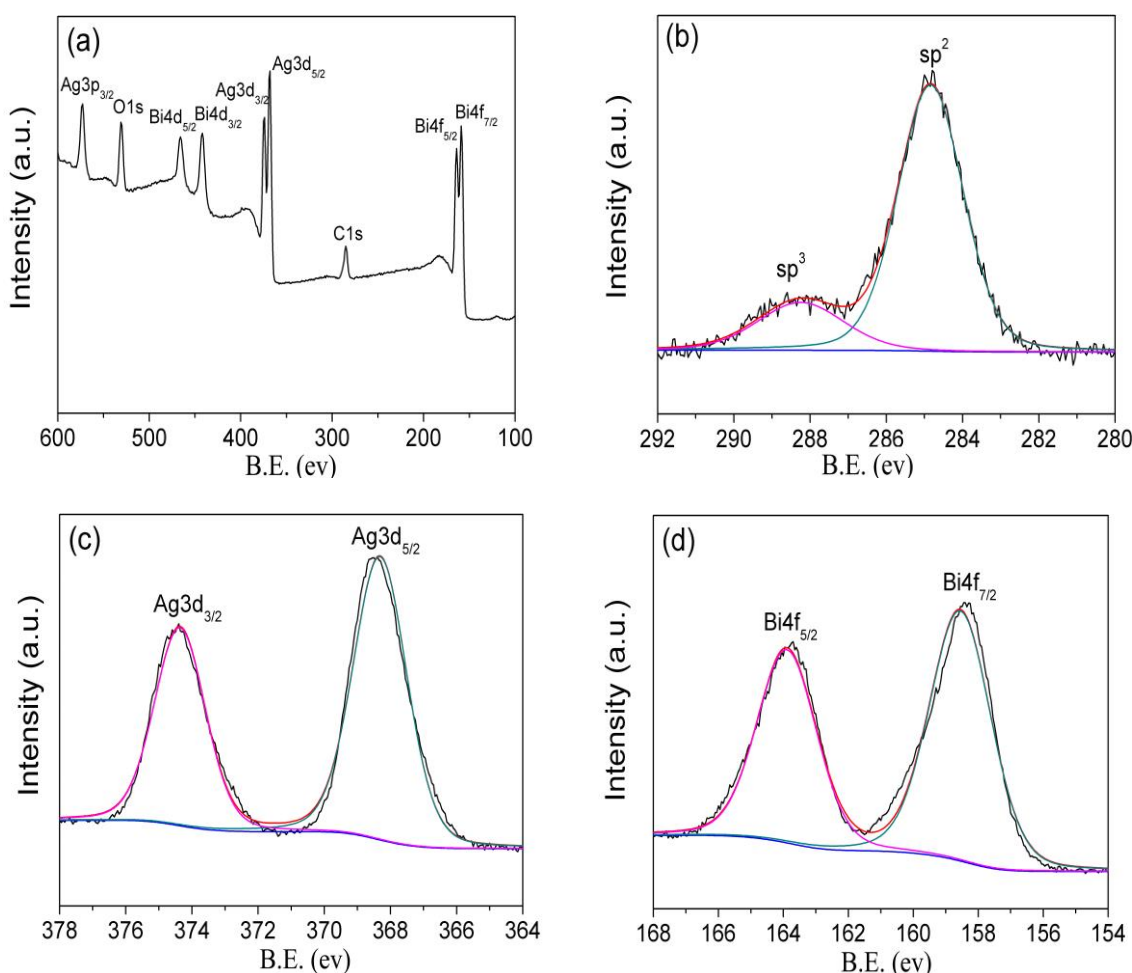

Figure 3. XPS full-spectrum(a) and fine-spectrum (b) C 1s, (c) Ag 3d and (d) Bi 4f of the ABO/GO sample

The XPS spectrum of an ABO/GO sample provided further evidence for the deposition of ABO onto GO (Fig. 3a). An asymmetric peak centered at 284.8 eV with an extended tail in the higher energy

region can be ascribed to sp^2-hybridized GO, as shown in Fig. 3b. Figure 3c shows that Ag 3d gives rise to two major peaks at binding energies of 368.18 and 374.17 eV, which can be attributed to Ag $3d_{5/2}$ and Ag $3d_{3/2}$, respectively, confirming the existence of Ag^+ [24,25]. Characteristic Bi $4f_{7/2}$ and $4f_{5/2}$ peaks can be observed at 158.63 and 163.92 eV, respectively (Fig. 3d), corresponding to Bi^{3+} [26].

*3.2 Electrochemical characterization and enhancement meachanims*
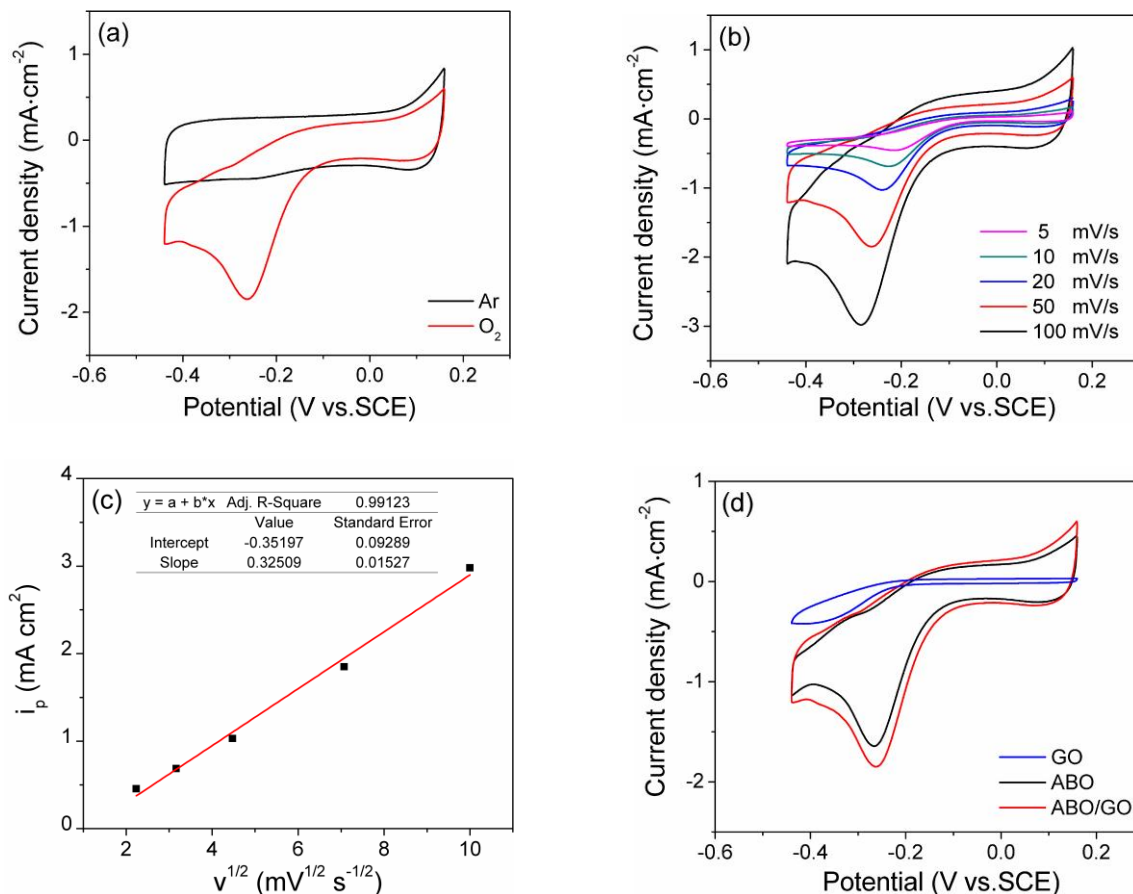
Figure 4. (a) CVs of ABO/GO at a scan rate of 50 mV·s^{-1} in a 0.1 mol·L^{-1} KOH solutions saturated with Ar and O$_2$, (b) CVs of ABO electrode at different scan rate, (c) Linear relationship between peak current and scan rate, and (d) The contrast of CVs at a scan rate of 50 mV·s^{-1} in 0.1 mol·L^{-1} KOH solutions saturated with O$_2$. (black: ABO/GO, red: ABO, green: GO).

The electrocatalytic activity of ABO/GO towards the ORR was firstly determined by Cyclic voltammograms (CVs) in KOH solutions (0.1 mol·L^{-1}) saturated with Ar and O$_2$ at a scan rate of 50 mV·s^{-1}. As shown in Fig. 4a, a strong reduction peak at about −0.26 V (vs. SCE) developed under oxygen atmosphere, no significant reaction was observed in argon atmosphere. This suggested that the ORR occurred on the surface of the ABO/GO electrocatalyst. Figure 3b shows the CVs of the ABO/GO acquired at different scan rates. It can be seen that on increasing the scan rate from 5 mV s^{-1} to 100 mV s^{-1}, the oxidation peak increased accordingly. As can be seen from Fig. 5c, the peak current i_p and scan rate $v^{1/2}$ showed a good linear relationship. For comparison, ABO and GO were also investigated. According to Fig. 5d, we found that the order of the reduction peak intensity was

ABO/GO > ABO > GO. The reason may be that the addition of GO as the carrier was added to ABO to form ABO/GO composite, increasing the area of electrochemical activity, further increasing the activity of the catalyst.

The rotating disk electrode (RDE) voltammetry of ABO/GO electrocatalyst for ORR was measured in O_2-saturated and Ar-saturated KOH (0.1 mol·L^{-1}) solutions at a scan rate of 5 mV s^{-1} are given in Fig. 5a, in which the seven curves substantially overlap at higher potentials E > −0.2 V. The ORR was slower and the speed of the rotating disk electrode had little effect on the reaction, indicating that the catalytic ORR of O_2 on the glassy carbon electrode surface was controlled by an electrochemical process at high potentials. At lower potentials E < −0.2 V, it was observed that the cathodic reduction current was related to the solubility of O_2 in the solution. On increasing the rotation speed of the electrode, the diffusion layer thickness of dissolved oxygen at the surface of the rotating disk electrode gradually decreased.
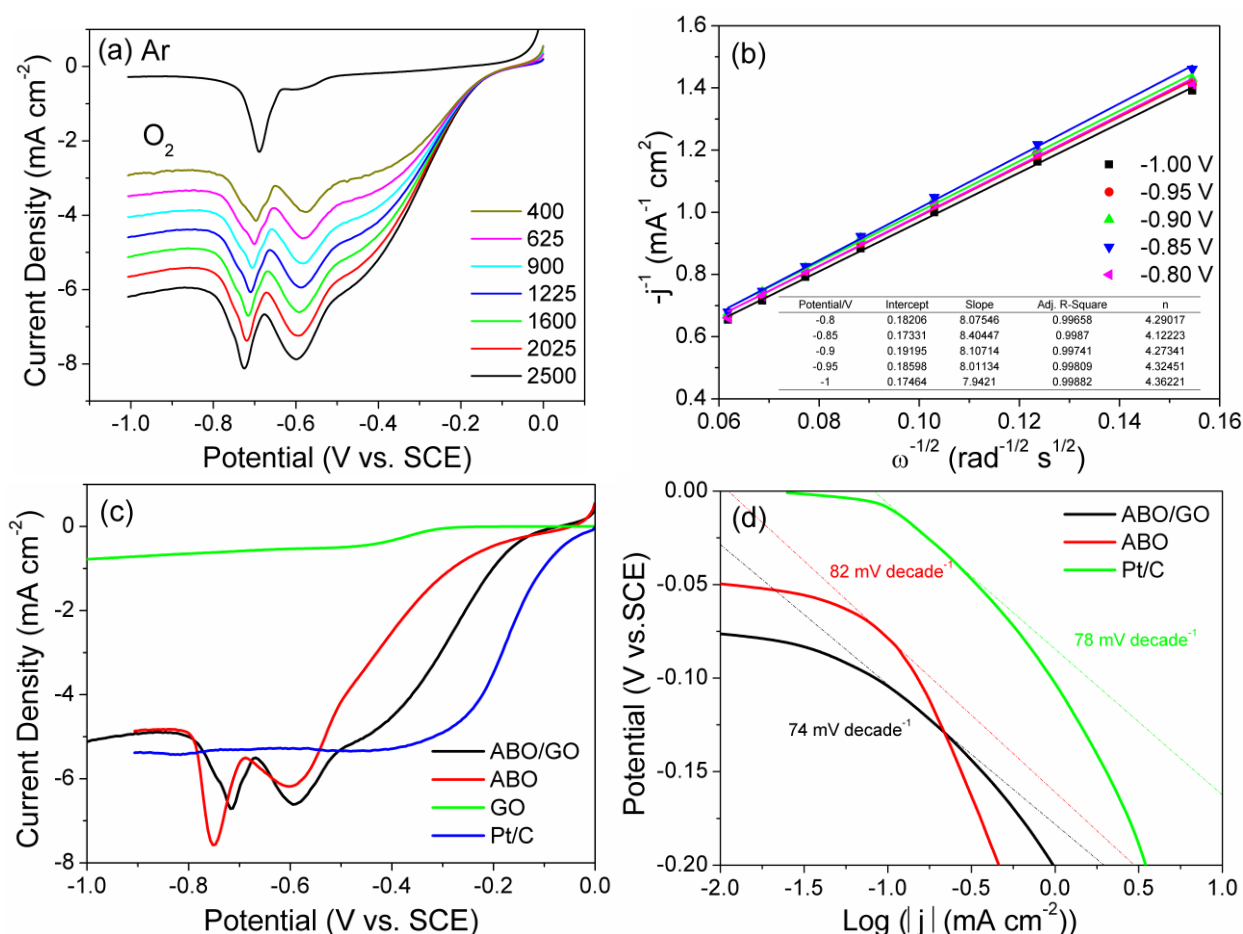
Figure 5. The rotating disk test for ABO/GO composite catalyst at different rotating rates (a) and the K-L plots for ABO/GO composite at different potentials (b), (c) LSV of the GO, ABO, ABO/GO and Pt/C, and (d) Tafel slope of the GO, ABO, ABO/GO and Pt/C.

The measurements revealed a linear relationship between the rate of rotation and the diffusion rate of oxygen on the catalyst surface. It can be seen that the oxygen reduction current density and rotation speed also showed a linearly increasing relationship at high polarization potentials, indicating

that the oxygen reduction current density was controlled by the liquid-phase diffusion of oxygen at potential range from −0.6 to −0.2 V. In addition, a strong reduction peak was found at −0.72 V, corresponding to the reduction of Bi(III)→Bi(0) in $Ag_4Bi_2O_5$, consistent with scanning experiments under Ar atmosphere [27].

The number of electrons transferred in the oxygen reduction process can be calculated by the Koutechy–Levich (K–L) equation as given by [28]: $i^{-1}=B+1/K \times 1/(\omega^{1/2})$, in which $K=0.62nFC_0D^{2/3}v^{-1/6}$, here i is the current density at the applied potential and ω is the electrode rotation rate (rpm). The parameter K at different applied voltages could be obtained from the slopes of the $-i^{-1}$ vs. $\omega^{1/2}$ plots in Fig. 5b. The values of i and ω were taken from the diffusion-controlled region in Fig. 5b. where n is the overall number of electrons transferred in ORR, F is the Faraday constant (96485 C·mol^{-1}), C_0 is the bulk concentration of O_2 (1.26×10^{-3} mol·L^{-1}), D is the diffusion coefficient of O_2 in 0.1 M KOH (1.93×10^{-5} cm^2·s^{-1}), and v is the kinetic viscosity (0.01 cm^2·s^{-1}). Figure 5b shows $-i^{-1}$ vs. $\omega^{1/2}$ plots for the $Ag_4Bi_2O_5$ catalyst from −0.8 V to −1.0 V. It can be seen that all of the curves showed good linearity at different potentials, and that the slopes remained almost unchanged, indicating that the ORR electron-transfer numbers were similar at different potentials. From these curves, the electron-transfer number was calculated as close to 4 at scanning potentials in the range from −0.8 V to −1.0 V. The LSV of GO, ABO, ABO/GO and Pt/C catalyst was investigated between 0.0 V and 1.0 V (vs. SCE) in O_2-saturated KOH (0.1 mol·L^{-1}) solutions at a scan rate of 5 mV s^{-1} at 1600 rpm, as shown in Fig. 5c. In contrast, ABO/GO catalyst exhibited good activity than GO and ABO, and got close to Pt/C catalyst under the same condition. The Tafel slope of ABO, ABO/GO and Pt/C is 82, 74 and 78mV per decade (Fig. 5d). The low ORR Tafel slope of ABO/GO implies a transition from Langmuirian adsorption to the Temkin adsorption of adsorbed O/OH groups [29]. Therefore, the electrochemical catalyst activation of ABO/GO is superior to GO and ABO, which isclose to that of Pt/C. This further indicates that ABO/GO composite has high ORR activity and stability.

4. CONCLUSION

A nano-$Ag_4Bi_2O_5$/graphene oxide (ABO/GO) composite has been synthesized by a co-precipitation method in which ABO was precipitated on the surface of suspended GO. Compared with pure ABO and GO, the ABO/GO composite demonstrated excellent catalytic performance and stability in the ORR and the process involved a four-electron pathway.

References

1. M. V. Kannan, G. Gnana kumar, *Biosens. Bioelectron*, 77 (2015) 1208-1220.

2. J. Wang, Z. X. Wu, L. L. Han, Y. Y. Liu, J. P. Guo, H. L. Xin and D. L. Wang, *Chin. Chem. Lett.*, 27 (2016) 597-601.
3. S. Park, R. S. Ruoff, *Nature Nanotech*, 5 (2009) 217-224.
4. H. He, J. Klinowski, M. Forster and A. Lerf, *Phys. Lett.*, 287 (1998) 53-56.
5. L. C. Chen, S. Lei, M. Z. Wang, J. Yang and X. W. Ge, *Chin. Chem. Lett.*, 27 (2016) 511-517.
6. K. Vinodgopal, B. Neppolian, I. V. Lightcap, F. Grieser, M. Ashokkumar and P. V. Kamat, *Carbon*, 49 (2011) 4731-4738.
7. Z. Xu, H. Gao and G. Hu, *Carbon*, 49 (2011) 4731-4738.
8. Y. Yu, Y. Li, Y. Pan and C. J. Liu, *Nanoscale Res. Lett.*, 7 (2012) 1-4.
9. S. H. Yu, G. C. Zhao, *Int. J. Electrochem.*, 6 (2012) 2090-2095.
10. J. J. Fang, S. F. Li, W. K. Zha, H. Y. Cong, J. F. Chen and Z. Z. Chen, *J. Inorg. Mater.*, 26 (2011) 467-471.
11. J. Lou, S. Jiang, H. Zhang, J. Jiang and X. Liu, *Anal. Chim. Acta.*, 709 (2012) 47-53.
12. J. Liu, H. Bai, Y. Wang, Z. Liu, X. Zhang and D. D. Sun, *Adv. Funct. Mater.,* 20 (2010) 4175-4181.
13. Z. Yin, S. Wu, X. Zhou, X. Huang, Q. Zhang, F. Boey and H. Zhang, *Small*, 6 (2010) 307-312.
14. J. Yan, Z. Fan, T. Wei, W. Qian, M. Zhang and F. Wei, *Carbon*, 48 (2010) 3825-3833.
15. F. Li, J. Song, H. Yang, S. Gan, Q. Zhang, D. Han, A. Ivaska and L. Niu, *Nanotechno.,* 20 (2009) 19748-19753.
16. M. Z. Kassaee, E. Motamedi, M. Majdi, *Chem. Eng. J.*, 172 (2011) 540-549.
17. P. Shi, X. Dai, H. Zheng, D. Li, W. Yao and C. Hu, *Chem. Eng. J.*, 240 (2014) 264-270.
18. M. Khan, A. B. Yousaf, M. Chen, C. Wei, X. Wu, N. Huang, Z. Qi and L. Li, *J. Power Sources*, 282 (2015) 520-528.
19. W. S. Hummers, R. E. Offeman, *J. Am. Chem. Soc.*, 80 (1958) 1339-1339.
20. L. Tang, Y. Wang, Y. Li, H. Feng, J. Lu and J. Li, *Adv. Funct. Mater.*, 19 (2009) 2782-2789.
21. S. Stankovich, D. A. Dikin, R. D. Piner, K. A. Kohlhaas, A. Kleinhammes, Y. Jia, Y. Wu, S. B. T. Nguyen, R. S. Ruoff, *Carbon*, 45 (2007) 1558-1565.
22. S. Guo, D. Wen, Y. Zhai, S. Dong and Erkang, *Acs Nano.*, 4 (2010) 3959-3968.
23. T. N. Lambert, C. A. Chavez, B. Hernandezsanchez, P. Lu, N. S. Bell, A. Ambrosini, T. Friedman, T. J. Boyle, D. R. Wheeler and D. L. Huber. *J. Phys. Chem.*, c4 (2009) 19812-19823.
24. M. A. Kostowskyj, D. W. Kirk and S. J. Thorpe, *Int. J. Hydrogen Energy*, 35 (2010) 5666-5672.
25. S. Deibele, M. Jansen, *J. Solid State Chem.*, 147 (1999) 117-121.
26. Wagner C D, Naumkin A V, Kraut-Vass A, et al. NIST X ray Photoelectron Spectroscopy Database (Version 3.5). http://srdata.nist.gov/xps.
27. J. Q. Pan, Q. Wang, Y. Z. Sun, Z. H. Wang, *Electrochim. Acta.*, 59 (2012) 515-521.
28. Z. H. Sheng, H. L. Gao, W. J. Bao, F. B. Wang and X. H. Xia, *J. Mater. Chem.*, 22 (2012) 390-395.
29. F. W. T. Goha, Z. L. Liu, X. M. Ge, Y. Zong, G. J. Du and T. S. A. Hora, *Electrochim. Acta,* 114 (2013) 598.